Analytical expressions for the longitudinal evolution of nondiffracting pulses truncated by finite apertures

Michel Zamboni-Rached

Department of Microwaves and Optics, Faculty of Electrical Engineering, State University of Campinas, (UNICAMP), Campinas, SP, Brasil

Received January 23, 2006; accepted February 14, 2006; posted March 24, 2006 (Doc. ID 67363)

Starting from some general and plausible assumptions based on geometrical optics and on a common feature of the truncated Bessel beams, a heuristic derivation is presented of very simple analytical expressions capable of describing the longitudinal (on-axis) evolution of axially symmetric nondiffracting pulses truncated by finite apertures. The analytical formulation is applied to several situations involving subluminal, luminal, or superluminal localized pulses, and the results are compared with those obtained by numerical simulations of the Rayleigh–Sommerfeld diffraction integrals. The results are in excellent agreement. The present approach can be rather useful, because it yields, in general, closed-form expressions, avoiding the need for time-consuming numerical simulations, and also because such expressions provide a powerful tool for exploring several important properties of the truncated localized pulses, such as their depth of fields, the longitudinal pulse behavior, and the decaying rates. © 2006 Optical Society of America

OCIS codes: 050.1220, 050.1960, 320.5550, 350.7420.

1. INTRODUCTION

Ideal nondiffracting pulses (INPs) are infinite-energy solutions of the ordinary linear wave equation, capable of maintaining their spatial shapes indefinitely (sometimes with just small local variations) while propagating.[1–9] When these ideal solutions are adapted to real situations and applications, they must be spatially truncated by a finite aperture (i.e., generated by a finite aperture), becoming transformed into finite-energy solutions with finite field depths, even if these field depths are very large when compared with those of ordinary pulses.

When we truncate an INP, the resulting wave field cannot be obtained, in general, in analytical form. In this case one has to resort to diffraction theory and perform numerical simulations of the diffraction integrals, such as the well-known Rayleigh–Sommerfeld formula.

Indeed, one can get very important pieces of information about a truncated nondiffracting pulse (TNP) by performing numerical simulations of its longitudinal evolution,[11–14] especially when the pulse is axially symmetric.

In this paper[15] it will be shown that, by using some general and plausible assumptions based on geometrical optics and on a common feature of truncated Bessel beams, a heuristic derivation of simple analytical expressions is possible, capable of furnishing the longitudinal (on-axis) evolution of the TNPs. It is interesting to note that this approach depends only on the spectral structure of the relevant INP.

The results of our analytical method, when applied to several different situations involving subluminal, luminal, or superluminal TNPs, are compared with the results obtained from the usual numerical simulation of the Rayleigh–Sommerfeld integrals: the results are in excellent agreement. This method, due to its extreme simplicity and analytical character, can be a powerful tool for exploring several important properties of the TNPs, such as their depth of fields, the longitudinal pulse behavior, and the decaying rates; for revealing the effects of the spectral parameters on the pulses evolution; and also for comparing the "effectiveness" of the different kinds of TNPs, such as subluminal, luminal, and superluminal. Without this method, all those results could be achieved (in each particular situation) only by performing several time-consuming numerical simulations.

2. HEURISTIC APPROACH FOR DESCRIBING THE ON-AXIS EVOLUTION OF A TRUNCATED NONDIFFRACTING PULSE

Let us begin this section by making some comments about the truncated Bessel beams and about some approximations that will be used below for developing the method proposed here.

A. Some Observations on and Approximations of Truncated Bessel Beams

An ideal (infinite-energy) Bessel beam (IBb) is given by [16]

$$\Psi_{\mathrm{IBb}}(\rho,z,t) = J_0(k_\rho \rho) e^{i\beta z} e^{-i\omega t}, \tag{1}$$

where $\rho^2 = x^2 + y^2$ is the transverse coordinate, $k_\rho = \sqrt{\omega^2/c^2 - \beta^2}$ is the transverse wavenumber, β is the longitudinal wavenumber, and ω is the angular frequency.

An important parameter[17–20] of an IBb is its axicon angle θ, where $\omega = c\beta/\cos\theta$. When a Bessel beam is truncated by a finite aperture of radius R, Eq. (1) cannot be used to describe the resulting beam in the whole space.[21,22] However, if the size of the aperture is large

enough to contain several bright rings of the ideal incident Bessel beam, i.e., if $R \gg 1/k_\rho$, we can use geometrical optics to get some characteristics of the truncated Bessel beam (TBb) evolution. In this case (see Fig. 1), we can say that, in the spatial region localized inside the cone oriented along the z axis, with apex at $z=Z=R/\tan\theta$ and base given by the circular aperture, the resulting TBb can be approximately described by Eq. (1).

However, when using geometrical optics, after the distance $Z=R/\tan\theta$, the on-axis amplitude of the TBb becomes approximately zero (see Fig. 1). The distance Z is called the depth field of the TBb.

Keeping the above observations in mind, one may affirm that, since $R \gg 1/k_\rho$, the on-axis behavior of a TBb can be approximately described by

$$\Psi_{\mathrm{TBb}}(\rho=0,z,t) \simeq \begin{cases} e^{i\beta z}e^{-i\omega t} & \text{for } z \leqslant \dfrac{R}{\tan\theta} \\ 0 & \text{for } z > \dfrac{R}{\tan\theta} \end{cases}, \qquad (2)$$

which can be compactly written as

$$\Psi_{\mathrm{TBb}}(\rho=0,z,t) \simeq e^{i\beta z}e^{-i\omega t}\left[H(z) - H\left(z - \frac{R}{\tan\theta}\right)\right], \qquad (3)$$

where $H(\cdot)$ is the Heaviside step function. Approximation (3) is the starting point for our heuristic method describing the on-axis TNP's behavior. According to approximation (3), the on-axis field intensity of a TBb is a rectangular function with unitary value, until $z=Z$.

On the other hand, when a numerical simulation of the diffraction integrals is performed,[8,16] one can observe that the TBb presents some on-axis field oscillations around the unitary value before suffering an abrupt decay after $z=Z$. Such oscillations cannot be predicted by geometrical optics and arise only as a result of the abrupt truncation made by the aperture. However, it is important to stress here that, despite the fact that those oscillations are not predicted by approximation (3), such an error *is not present*, in general, in the case of our description of truncated localized pulses. One can understand this by noting that, since nondiffracting pulses are constructed through Bessel beam superpositions, those oscillations, originating from each TBb, suffer a destructive interference.

With all this in mind, we are ready to develop our method.

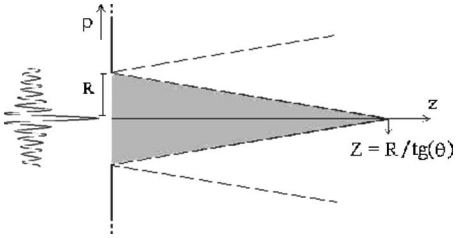

Fig. 1. Typical Bessel beam truncated by a finite aperture.

B. Heuristic Approach

It is well known[1–9] that axially symmetric ideal nondiffracting pulses (INPs) can be made by zero-order Bessel beam superpositions,

$$\Psi(\rho,z,t) = \int_0^\infty \mathrm{d}\omega \int_{-\omega/c}^{\omega/c} \mathrm{d}\beta \bar{S}(\omega,\beta) J_0\left(\rho\sqrt{\frac{\omega^2}{c^2}-\beta^2}\right) e^{i\beta z}e^{-i\omega t} \qquad (4)$$

provided that the spectral function $\bar{S}(\omega,\beta)$ entails a linear relationship of the type

$$\omega = V\beta + b \qquad (5)$$

between ω and β. In this way, by putting $\bar{S}(\omega,\beta) = S(\omega)\delta(\omega - V\beta - b)$, the general form of an axially symmetric INP is written as

$$\Psi_{\mathrm{INP}}(\rho,z,t) = e^{-ibz/V}\int_{\omega_{min}}^{\omega_{\max}} d\omega S(\omega) \times J_0\left(\rho\sqrt{\left(\frac{1}{c^2}-\frac{1}{V^2}\right)\omega^2 + \frac{2b\omega}{V^2} - \frac{b^2}{V^2}}\right) e^{i\omega\zeta/V}, \qquad (6)$$

where $\zeta = z - Vt$, V is the peak velocity and $S(\omega)$ is the frequency spectrum. Obviously, the INP will be subluminal, luminal or superluminal, depending on the value of V, it being less than equal to, or greater than c. The positive quantities ω_{min} and $\omega_{\max}$ are the minimum and maximum angular frequency allowed for the Bessel beams in the superposition (6), and their values have to be estimated as follows.

Once we have chosen the value of V in Eq. (6), the values of b, ω_{min}, and $\omega_{\max}$ are interrelated in such a way that

$$k_\rho^2 = \left(\frac{1}{c^2}-\frac{1}{V^2}\right)\omega^2 + \frac{2b\omega}{V^2} - \frac{b^2}{V^2} \geqslant 0, \qquad \beta \geqslant 0, \qquad (7)$$

for all positive angular frequency $\omega_{min} \leqslant \omega \leqslant \omega_{\max}$ used in superposition (6).

In relation (7), the condition on k_ρ eliminates any nonphysical behaviors of Bessel functions and evanescent waves in Eq. (6). The second condition ($\beta \geqslant 0$) eliminates any backward-traveling Bessel beams in the same superposition, since we are considering positive values of the angular frequency only.

Taking into account conditions (7), one has

- For subluminal ($V<c$) INPs: $b>0$, $\omega_{min}=b$ and $\omega_{\max}=cb/(c-V)$.
- For luminal ($V=c$) INPs: $b>0$, $\omega_{min}=b$ and $\omega_{\max}=\infty$.
- For superluminal ($V>c$) INPs: $b \geqslant 0$, $\omega_{min}=b$ and $\omega_{\max}=\infty$. Or $b<0$, $\omega_{min}=cb/(c-V)$ and $\omega_{\max}=\infty$.

The INPs provided by Eq. (6) can propagate without distortion indefinitely, with peak velocity V. Such INPs possess infinite energy, and so, for real applications, they must be spatially truncated (i.e., generated by finite apertures),[11–14] resulting in finite-energy solutions, with a finite depth of field. When such truncation is made, the resulting pulse in general cannot be obtained in an ana-

lytical form but has to be numerically calculated from diffraction theory by using, for example, the Rayleigh–Sommerfeld formula.[10–14] That is, once we have a known INP solution Ψ_{INP}, its truncated version Ψ_{TNP}, generated by a finite aperture of radius R on the plane $z=0$, results in

$$\Psi_{\mathrm{TNP}}(\rho,z,t)=\int_0^{2\pi}\mathrm{d}\phi'\int_0^R\mathrm{d}\rho'\rho'\frac{1}{2\pi D}\left\{[\Psi_{\mathrm{INP}}]\frac{(z-z')}{D^2}+[\partial_{ct'}\Psi_{\mathrm{INP}}]\frac{(z-z')}{D}\right\},\tag{8}$$

the quantities enclosed by the square brackets being evaluated at the retarded time $ct'=ct-D$. The distance $D=[(z-z')^2+\rho^2+\rho'^2-2\rho\rho'\cos(\phi-\phi')]^{1/2}$ is the separation between the source and the observation points. Due to its complexity, Eq. (8) has to be solved numerically in most cases.

Of particular interest is the on-axis behavior of Ψ_{TNP}. Actually, much important information can be extracted from the evolution of $\Psi_{\mathrm{TNP}}(\rho=0,z,t)$, such as its depth of field, the pulse decaying rate, and the effects of the different spectral parameters on the pulse evolution; and, even more important, the quantity $\Psi_{\mathrm{TNP}}(\rho=0,z,t)$ can be used to compare the performance of different kinds of TNPs, such as, for example, the luminal and the superluminal ones.

On considering axially symmetric TNPs and making $\rho=0$ in Eq. (8), we get some simplifications, because the integration on ϕ' can be done immediately. But, even in this case, the integration on ρ' rarely can be carried out analytically, due to the complexity of the integrand, and numerical simulations are once more required.

To overcome this problem, let us propose the following heuristic approach: First, we consider the Bessel beam superposition (6), which provides us with the INPs. Second, we make the assumption that each Bessel beam, with frequency ω and axicon angle $\theta(\omega)$, entering in superposition (6), obeys the following condition,

$$R\gg\frac{1}{k_\rho}=\frac{c}{\omega\sin\theta(\omega)},\tag{9}$$

R being the radius of the finite aperture that will be used for truncating the INP. The above assumption is very plausible, since efficient TNPs are generated by large apertures.

Once condition (9) is fulfilled by all Bessel beams in superposition (6), we can use again geometrical optics and assume that, after the truncation, the on-axis behavior of each one of those Bessel beams can be approximated by approximation (3).

Third, taking into account relations (3) and (6), we may conjecture that the on-axis evolution of the *truncated* nondiffracting pulse is approximately given by

$$\Psi_{\mathrm{TNP}}(\rho=0,z,t)\simeq e^{-ibz/V}\int_{\omega_{min}}^{\omega_{\max}}\mathrm{d}\omega S(\omega)\times e^{i\omega\zeta/V}\left[H(z)-H\left(z-\frac{R}{\tan\theta(\omega)}\right)\right],\tag{10}$$

where $H(\cdot)$ is the Heaviside step function and, let us recall, $\theta(\omega)$ is the axicon angle of the Bessel beam with angular frequency ω. We should note that in the integrand of approximation (10), the step function $H(z-R/\tan\theta(\omega))$ depends on ω, through of $\theta(\omega)$.

We can rewrite approximation (10) in the form

$$\Psi_{\mathrm{TNP}}(\rho=0,z>0,t)\simeq e^{-ibz/V}\left[\int_{\omega_{min}}^{\omega_{\max}}S(\omega)e^{i\omega\zeta/V}\mathrm{d}\omega-\int_{\omega_{min}}^{\omega_{\max}}S(\omega)e^{i\omega\zeta/V}H\left(z-\frac{R}{\tan\theta(\omega)}\right)\mathrm{d}\omega\right],\tag{11}$$

where the first term on the right-hand side of approximation (11) is nothing but the INP $\Psi_{\mathrm{INP}}(\rho=0,z,t)$, while the second term is the perturbation due to the truncation.

Now, remembering that for a Bessel beam of axicon angle θ we have $\omega=c\beta/\cos\theta$ and that the spectra of INPs impose the constraint $\omega=V\beta+b$ between angular frequencies and longitudinal wavenumbers, it becomes easy to show that

$$\frac{R}{\tan\theta(\omega)}=\frac{R}{\sqrt{1-(c/V-bc/V\omega)^2}}\left(\frac{c}{V}-\frac{bc}{V\omega}\right)\tag{12}$$

and thus

$$H\left(z-\frac{R}{\tan\theta(\omega)}\right)=H\left(z-\frac{R(c/V-bc/V\omega)}{\sqrt{1-(c/V-bc/V\omega)^2}}\right)=\begin{cases}1 & \text{for } z\geqslant\dfrac{R(c/V-bc/V\omega)}{\sqrt{1-(c/V-bc/V\omega)^2}}\\ 0 & \text{for } z<\dfrac{R(c/V-bc/V\omega)}{\sqrt{1-(c/V-bc/V\omega)^2}}\end{cases}.\tag{13}$$

With all that preceded, we can finally write

$$\Psi_{\mathrm{TNP}}(\rho=0,z,t)\simeq e^{-ibz/V}\left[\int_{\omega_{min}}^{\omega_{\max}}S(\omega)e^{i\omega\zeta/V}\mathrm{d}\omega-\int_{\omega_{min}}^{\omega_{\max}}S(\omega)e^{i\omega\zeta/V}H\left(z-\frac{R(c/V-bc/V\omega)}{\sqrt{1-(c/V-bc/V\omega)^2}}\right)\mathrm{d}\omega\right].\tag{14}$$

In the next subsection, we will analyze the fundamental Eq. (14) for the three possible types of TNPs: subluminal, luminal, and superluminal.

1. Subluminal Truncated Nondiffracting Pulse

For the subluminal pulses ($V<c$), we have $b>0$, $\omega_{min}=b$ and $\omega_{\max}=cb/(c-V)$. In this way, taking into account these facts, and that $z\geqslant 0$ and $\omega_{\min}\leqslant\omega\leqslant\omega_{\max}$, we can show, after several manipulations, that Eq. (13) can be written as

$$H\left(z-\frac{R(c/V-bc/V\omega)}{\sqrt{1-(c/V-bc/V\omega)^2}}\right)=\begin{cases}1 & \text{for } \omega\leqslant bc \\ 0 & \text{for } \omega>bc\end{cases}\Bigg/\left(c-\frac{zV}{\sqrt{z^2+R^2}}\right). \tag{15}$$

Now, by noting that $\omega_{\min}=b<bc/(c-zV/\sqrt{z^2+R^2})<\omega_{\max}=bc/(c-V)$, one can write Eq. (14) for the *subluminal* case as

$$\Psi_{\mathrm{TNP}}(\rho=0,z>0,t)\simeq e^{-ibz/V}\left[\int_b^{bc/(c-V)}S(\omega)e^{i\omega\zeta/V}\mathrm{d}\omega-\int_b^{bc/(c-zV/\sqrt{z^2+R^2})}S(\omega)e^{i\omega\zeta/V}\mathrm{d}\omega\right]=e^{-ibz/V}\left[\int_{bc/(c-zV/\sqrt{z^2+R^2})}^{bc/(c-V)}S(\omega)e^{i\omega\zeta/V}\mathrm{d}\omega\right], \tag{16}$$

which represents our method in the case of *subluminal* TNPs. It is a very simple equation, capable of providing closed-form, analytical results for several different frequency spectra $S(\omega)$, as we shall see in Section 3.

2. Luminal Truncated Nondiffracting Pulse

For luminal TNPs ($V=c$), we have $b>0$, $\omega_{\min}=b$, and $\omega_{\max}=\infty$. With this, and taking into account that $z\geqslant 0$ and $\omega_{\min}\leqslant\omega\leqslant\omega_{\max}$, we can, after several manipulations, show that Eq. (13) may be written as

$$H\left(z-\frac{R(c/V-bc/V\omega)}{\sqrt{1-(c/V-bc/V\omega)^2}}\right)=\begin{cases}1 & \text{for } \omega\leqslant b \\ 0 & \text{for } \omega>b\end{cases}\Bigg/\left(1-\frac{z}{\sqrt{z^2+R^2}}\right), \tag{17}$$

and, by noting that $\omega_{\min}=b<b/(1-z/\sqrt{z^2+R^2})<\omega_{\max}=\infty$, we can write approximation (14), for the *luminal* case, as

$$\Psi_{\mathrm{TNP}}(\rho=0,z>0,t)\simeq e^{-ibz/c}\left[\int_b^{\infty}S(\omega)e^{i\omega\zeta/c}\mathrm{d}\omega-\int_b^{b/(1-z/\sqrt{z^2+R^2})}S(\omega)e^{i\omega\zeta/c}\mathrm{d}\omega\right]=e^{-ibz/c}\left[\int_{b/(1-z/\sqrt{z^2+R^2})}^{\infty}S(\omega)e^{i\omega\zeta/c}\mathrm{d}\omega\right]. \tag{18}$$

Equation (18), which represents our method in the case of *luminal* TNPs, is very simple too and can provide closed-form, analytical results for many different frequency spectra $S(\omega)$, as we shall see in Section 3.

3. Superluminal Truncated Nondiffracting Pulse

For superluminal TNPs ($V>c$), the value of b, in the the spectral constraint (5), can assume negative or positive values, i.e., $-\infty\leqslant b\leqslant\infty$. Let us analyze the superluminal case of relations (13) and (14) for both situations, $b<0$ and $b\geqslant 0$.

Superluminal case for $b<0$. In this case, we have $\omega_{\min}=cb/(c-V)$ and $\omega_{\max}=\infty$. Taking into account that $z\geqslant 0$ and $\omega_{\min}\leqslant\omega\leqslant\omega_{\max}$, and, again, after several manipulations, we can show that for this case Eq. (13) can be written as

$$H\left(z-\frac{R(c/V-bc/V\omega)}{\sqrt{1-(c/V-bc/V\omega)^2}}\right)=\begin{cases}1 & \text{for } \omega\leqslant bc \\ 1 & \text{for } \omega\geqslant bc \\ 0 & \text{otherwise}\end{cases}\Bigg/\left(c-\frac{zV}{\sqrt{z^2+R^2}}\right)\begin{matrix}\text{and } z\leqslant\dfrac{R}{\sqrt{V^2/c^2-1}} \\ \text{and } z\geqslant\dfrac{R}{\sqrt{V^2/c^2-1}}\end{matrix}. \tag{19}$$

By noting that, when $z\leqslant R/\sqrt{V^2/c^2-1}$, we have $bc/(c-zV/\sqrt{z^2+R^2})\leqslant 0$ and that, when $z\geqslant R/\sqrt{V^2/c^2-1}$, we have $bc/(c-zV/\sqrt{z^2+R^2})>\omega_{\min}=bc/(c-V)$, one can write approximation (14), for the case $V>c$ and $b<0$, as

$$\Psi_{\mathrm{TNP}}(\rho=0,z>0,t)\simeq\begin{cases}e^{-ibz/V}\displaystyle\int_{bc/(c-V)}^{\infty}S(\omega)e^{i\omega\zeta/V}\mathrm{d}\omega & \text{for } z\leqslant\dfrac{R}{\sqrt{V^2/c^2-1}} \\ e^{-ibz/V}\displaystyle\int_{bc/(c-V)}^{bc/(c-zV/\sqrt{z^2+R^2})}S(\omega)e^{i\omega\zeta/V}\mathrm{d}\omega & \text{for } z\geqslant\dfrac{R}{\sqrt{V^2/c^2-1}}\end{cases}. \tag{20}$$

Approximation (20) represents our method in the case of *superluminal* TNPs *with* $b<0$. Again, the integrals are very simple and can provide closed-form, analytical results for many spectra $S(\omega)$.

Before going on to the next case, one can immediately see from approximation (20) that, independently of $S(\omega)$, the superluminal TNPs with $b<0$ will reach the distance $z=R/\sqrt{V^2/c^2-1}$ without deforming.

Superluminal case for $b\geqslant 0$. In this case, we have $\omega_{\min}=b$ and $\omega_{\max}=\infty$. Remembering that $z\geqslant 0$ and $\omega_{\min}\leqslant\omega\leqslant\omega_{\max}$ and, as before, after several manipulations, we can show that in this case Eq. (13) can be written in the same form of Eq. (19).

Now, taking into account that, when $z\leqslant R/\sqrt{V^2/c^2-1}$, it is $\omega_{\min}=b\leqslant bc/(c-zV/\sqrt{z^2+R^2})\leqslant\omega_{\max}=\infty$ and that, when $z>R/\sqrt{V^2/c^2-1}$, one has $bc/(c-zV/\sqrt{z^2+R^2})<0$, we can write our fundamental approximation (14), for the case $V>c$ and $b\geqslant 0$, in the form

$$\Psi_{\mathrm{TNP}}(\rho=0,z>0,t)\simeq\begin{cases} e^{-ibz/V}\displaystyle\int_{bc/(c-zV/\sqrt{z^2+R^2})}^{\infty} S(\omega)e^{i\omega\zeta/V}\mathrm{d}\omega & \text{for } z\leqslant\dfrac{R}{\sqrt{V^2/c^2-1}} \\ 0 & \text{for } z\geqslant\dfrac{R}{\sqrt{V^2/c^2-1}} \end{cases}. \tag{21}$$

Approximation (21) represents our method in the case of *superluminal* TNPs *with* $b\geqslant 0$. Again, many closed-form results, for many different spectra $S(\omega)$, can be obtained from approximation (21). We can also notice from approximation (21) that, for $V>c$ and $b\geqslant 0$, the superluminal TNPs will have very low intensities after the distance $z=R/\sqrt{V^2/c^2-1}$.

It is important to note that in our method, given by approximations (16), (18), (20), and (21), the on-axis evolution of a TNP depends only on the frequency spectrum $S(\omega)$ of its corresponding INP Ψ_{INP}, at variance with the Rayleigh–Sommerfeld formula (8), which depends on the mathematical expression of Ψ_{INP}.

Now we shall go on to Section 3, where our method will be applied to some important kinds of localized waves, and our results will be compared with those obtained by making numerical simulations with the Rayleigh–Sommerfeld formula.

3. APPLICATION TO SOME IMPORTANT CASES: CLOSED-FORM, ANALYTICAL RESULTS, AND THEIR COMPARISON WITH NUMERICAL SIMULATIONS OF THE RAYLEIGH–SOMMERFELD FORMULA

The method we have developed in Section 2 is described by approximations (16), (18), and (20)–(21), for the cases of truncated subluminal, luminal, and superluminal pulses, respectively. We shall now apply this method to some important cases involving TNPs, and it will be shown that the results agree very well with those obtained through numerical simulations of the Rayleigh–Sommerfeld formula (8).

A. The Method Applied to a Truncated Subluminal Pulse

A well known ideal subluminal ($V<c$) nondiffracting pulse[23] is

$$\Psi_{\mathrm{INP}}(\rho,z,t)=\exp\left(\frac{ibV\gamma^2\eta}{c^2}\right)\mathrm{sinc}\left(\frac{b\gamma}{c}\sqrt{\rho^2+\gamma^2\zeta^2}\right), \tag{22}$$

where $\gamma=1/\sqrt{1-V^2/c^2}$, $\eta=z-c^2t/V$, and, as always, $\zeta=z-Vt$.

Now, we want to describe the on-axis behavior of the *truncated* version (Ψ_{TNP}) of the the ideal solution (22). The subluminal INP [Eq. (22)] is generated by superposition (6), with a constant spectrum $S(\omega)=c/(2bV\gamma^2)$. However, we must note that this solution possesses backward-traveling components: Actually, it has $\omega_{\min}=bc/(c+V)$ instead of $\omega_{\min}=b$ [which ensures forward components only in superposition (6), as we have seen in Section 2]. It is the price paid to get such a closed-form and exact INP solution.

In any case, we may, and we must, minimize the contribution of those "backward" components by choosing the subluminal velocity V in such a way that $(c+V)/(c-V)\gg 1$. Once this condition is satisfied, we can observe that the INP [Eq. (22)] is then similar to that which would be obtained with the same $S(\omega)$, but with $\omega_{\min}=b$.

It should be noted that the comments and observations above have nothing to do with our method, which is constructed from the beginning in order to encompass causal (forward) solutions only and can be used for any values of the velocity V. Those remarks were made just in order that a causal behavior of the INP [Eq. (22)] be guaranteed.

Now, on using $S(\omega)=c/(2bV\gamma^2)$ in approximation (16), which describes the on-axis evolution of the subluminal TNPs, one gets

$$\begin{aligned}\Psi_{\mathrm{TNP}}(\rho=0,z>0,t)&\simeq\frac{c}{2bV\gamma^2}e^{-ibz/V}\left[\int_{bc/(c-zV/\sqrt{z^2+R^2})}^{bc/(c-V)}e^{i\omega\zeta/V}\mathrm{d}\omega\right]\\&=\frac{cV}{2bV\gamma^2 i\zeta}e^{-ibz/V}\left\{\exp\left[\frac{ibc}{V(c-V)}\zeta\right]-\exp\left[\frac{ibc\sqrt{z^2+R^2}}{V(c\sqrt{z^2+R^2}-zV)}\zeta\right]\right\},\end{aligned} \tag{23}$$

which is a very simple closed-form, analytical expression.

First, we use approximation (23) to get the pulse-peak intensity behavior. To do this, we just put $z=Vt\rightarrow\zeta=0$ in approximation (23).

Let us consider three different cases: (1) $V=0.995c$ and $b=1.5\times10^{15}$ Hz, (2) $V=0.998c$ and $b=6\times10^{14}$ Hz, and (3) $V=0.9992c$ and $b=2.4\times10^{14}$ Hz. In all three cases, we consider the radius of the finite aperture to be $R=4$ mm. At the same time, we compare our result with that obtained by the numerical simulation of the Rayleigh–Sommerfeld formula (8), with Ψ_{INP} given by Eq. (22).

In Fig. 2, plots represented by thin solid curves were obtained from approximation and (23), those represented by dotted curves come from the numerical simulation of Eq. (8). We can verify the excellent agreement existing among those results.

Now, we are interested in the on-axis longitudinal pulse evolution in the three cases considered above, in the time instants given by $t'=0.11$ ns, $t''=0.22$ ns and $t'''=0.33$ ns. Figures 3(a)–3(c) show the results corresponding to cases (1), (2), and (3), respectively. As above, the continuous curves represent the results obtained from approximation (23), and the dotted ones represent those coming from the numerical simulation of Eq. (8). Again, we consider $R=4$ mm. We can observe, once more, very good agreement among the results, confirming that our method works very well.

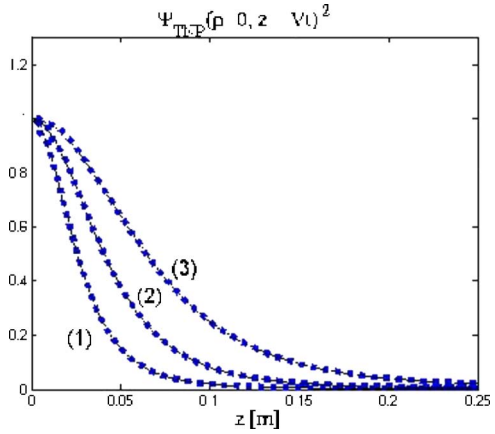

Fig. 2. Peak intensity evolution of the subluminal TNP for the three cases: (1) $V=0.995c$ and $b=1.5\times10^{15}$ Hz, (2) $V=0.998c$ and $b=6\times10^{14}$ Hz, (3) $V=0.9992c$ and $b=2.4\times10^{14}$ Hz. In all cases $R=4$ mm. The continuous curves represent results obtained from our closed-form analytical expression (23), and dotted curves represent results from the numerical simulation of the Rayleigh–Sommerfeld formula (8).

B. The Method Applied to the Truncated Luminal Focus Wave Mode Pulse

A very well known ideal luminal ($V=c$) nondiffracting pulse[1] is the focus wave mode pulse (FWM), given by

$$\Psi_{INP}(\rho,z,t)=\frac{ac}{ac-i\zeta}\exp\left(\frac{-ib}{2c}\eta\right)\exp\left[\frac{-b\rho^2}{2c(ac-i\zeta)}\right], \tag{24}$$

where $\eta=z+ct$, $\zeta=z-ct$, and $a>0$ is a constant.

Like all the INPs, the FWM possesses infinite energy and must be truncated (i.e., generated by a finite aperture) for real applications. We shall use our method to get closed-form, analytical expressions for the on-axis evolution of the truncated version Ψ_{TNP} of Eq. (24).

The exact ideal solution (24) is obtained from superposition (6) with $V=c$ and $S(\omega)=a\exp(ab/2)\exp(-a\omega)$. Because it has $\omega_{min}=b/2$, instead of $\omega_{min}=b$, its spectrum possesses backward components[1–6] in the range $b/2\leqslant\omega<b$. To overcome this problem, we must minimize the contribution of the nonphysical part of the spectrum; this can be done if $ab\ll1$. Once such a condition is obeyed, the INP [Eq. (24)] can be considered similar to the one that we would obtain with the same frequency spectrum of the FWM but with $\omega_{min}=b$. Again, let us note that such remarks are made just to validate the causality of the INP [Eq. (24)] and have nothing to do with our own method.

Now, by using $S(\omega)=a\exp(ab/2)\exp(-a\omega)$ in approximation (18), we get the on-axis evolution of the truncated FWM:

$$\Psi_{TNP}(\rho=0,z>0,t)\simeq a\,e^{ab/2}e^{-ibz/c}\int_{b/(1-z/\sqrt{z^2+R^2})}^{\infty}e^{-a\omega}e^{i\omega\zeta/c}d\omega$$
$$=\frac{ac}{ac-i\zeta}e^{ab/2}e^{-ibz/c}$$
$$\times\exp\left[\frac{-b\sqrt{z^2+R^2}(ac-i\zeta)}{c(\sqrt{z^2+R^2}-z)}\right], \tag{25}$$

which is a very simple closed-form, analytical expression.

First, let us put $\zeta=0$ into approximation (25) to get the pulse-peak intensity behavior. We consider three different

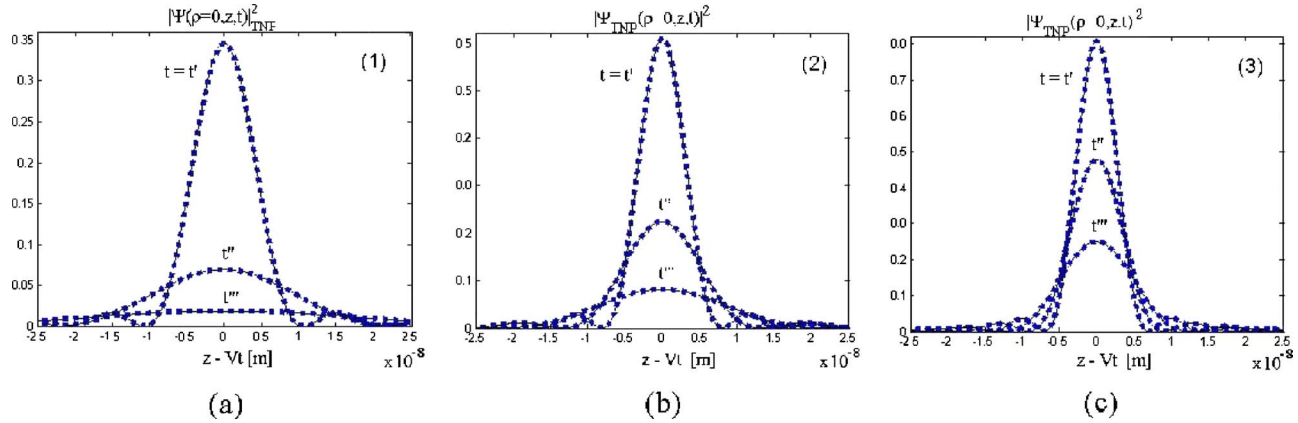

Fig. 3. On-axis evolution of the subluminal TNP, at the times $t'=0.11$ ns, $t''=0.22$ ns, and $t'''=0.33$ ns, for each case cited in Fig. 2; (a), (b), and (c), represent cases (1), (2), and (3), respectively. The continuous curves are the results obtained from our closed-form analytical expression (23) and dotted curves represent results from the numerical simulation of the Rayleigh–Sommerfeld formula (8).

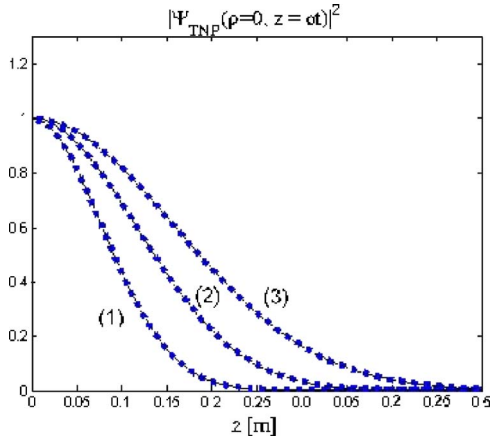

Fig. 4. Peak-intensity evolution of the truncated luminal FWM pulse for the three cases: (1) $a=1.6\times10^{-16}$ and $b=5\times10^{11}$ Hz, (2) $a=1.25\times10^{-16}$ s and $b=3\times10^{11}$ Hz, (3) $a=1\times10^{-16}$ and $b=2\times10^{11}$ Hz. In all cases $R=2$ mm. The continuous curves are the results obtained from our closed-form analytical expression (25) and dotted curves represent results from the numerical simulation of the Rayleigh–Sommerfeld formula (8).

cases: (1) $a=1.6\times10^{-16}$ s and $b=5\times10^{11}$ Hz, (2) $a=1.25\times10^{-16}$ s and $b=3\times10^{11}$ Hz, and (3) $a=1\times10^{-16}$ s and $b=2\times10^{11}$ Hz. In all cases we adopt the aperture radius $R=2$ mm.

Figure 4 shows the results. The continuous curves represent the results obtained from our approximation (25), and the dotted ones are the results of the numerical simulation of the Rayleigh–Sommerfeld formula (8). The results agree so well that the corresponding continuous and dotted curves superpose to each other.

Now, we are going to use approximation (25) to show the on-axis evolution of this TNP, in the three cases considered above, for the time instants $t'=0.22$ ns, $t''=0.44$ ns, and $t'''=0.66$ ns.

Figures 5(a)–5(c) show the results corresponding to cases (1), (2), and (3), respectively. The continuous curves are the results obtained from approximation (25), and the dotted curves are those coming from the numerical simulation of (8). Again, we consider $R=2$ mm. The results are in excellent agreement, showing the very good efficiency of the method.

C. The Method Applied to the Truncated Superluminal Focus-Wave Mode Pulse

An interesting, approximated, superluminal ($V>c$) ideal nondiffracting solution to the wave equation is the so-called[6] superluminal focus-wave-mode pulse (SFWM):

$$\Psi_{\mathrm{INP}}(\rho,z,t)=aV\exp\left(\frac{-ib}{2V}\eta\right)X\exp\left\{\frac{b(V^2+c^2)}{2V(V^2-c^2)}\times[(aV-i\zeta)-X^{-1}]\right\},\tag{26}$$

where $\eta=z+Vt$, $\zeta=z-Vt$, $a>0$ is a constant and where

$$X=\left[(aV-i\zeta)^2+\left(\frac{V^2}{c^2}-1\right)\rho^2\right]^{-1/2}.\tag{27}$$

Expression (26) is a very good approximate solution of the wave equation if $ab\ll1$, which is also the condition for minimizing the contribution of the backward components of expression (6). Actually, this superluminal INP can be obtained from superposition (6), with $b>0$, when using $S(\omega)=a\exp(ab/2)\exp(-a\omega)$, with constant $a>0$, but with $\omega_{\min}=b/2$ instead of $\omega_{\min}=b$.

To get the closed-form, analytical mathematical expression that describes the on-axis evolution of the truncated version of Eq. (26), let us put $S(\omega)=a\exp(ab/2)\exp(-a\omega)$ in approximation (21):

$$\Psi_{\mathrm{TNP}}(\rho=0,z>0,t)\simeq\begin{cases}\dfrac{aVe^{ab/2}e^{-ibz/V}}{aV-i\zeta}\exp\left[\dfrac{-bc\sqrt{z^2+R^2}(aV-i\zeta)}{V(c\sqrt{z^2+R^2}-zV)}\right] & \text{for } z\leqslant\dfrac{R}{\sqrt{V^2/c^2-1}}\\ 0 & \text{for } z\geqslant\dfrac{R}{\sqrt{V^2/c^2-1}}\end{cases},\tag{28}$$

Now, let us set $\zeta=0$ in approximation (28) to analyze the peak-intensity behavior of the truncated SFWM.

We consider three different cases: (1) $V=1.0002c$, $b=3\times10^{12}$ Hz, and $a=2.5\times10^{-17}$ s; (2) $V=1.0001c$, $b=1\times10^{12}$ Hz, and $a=5\times10^{-17}$ s; and (3) $V=1.00008c$, $b=2\times10^{12}$ Hz, and $a=1.1\times10^{-17}$ s. In all these cases we choose $R=3$ mm as being the radius of the aperture.

The plots are shown in Fig. 6, where the continuous curves represent our results using approximation (28), and the dotted ones represent those obtained from the numerical simulation of the Rayleigh–Sommerfeld formula (8). We can observe an excellent agreement among the results.

Now, we are going to use our method to show the on-axis evolution of the pulse intensity at three different times $t'=0.14$ ns, $t''=0.29$ ns, and $t'''=0.43$ ns, for each of the cases cited above.

Figures 7(a)–7(c) show the plots. Again, the curves given by continuous curves come from approximation (28) and the dotted ones from the numerical simulation of Eq.

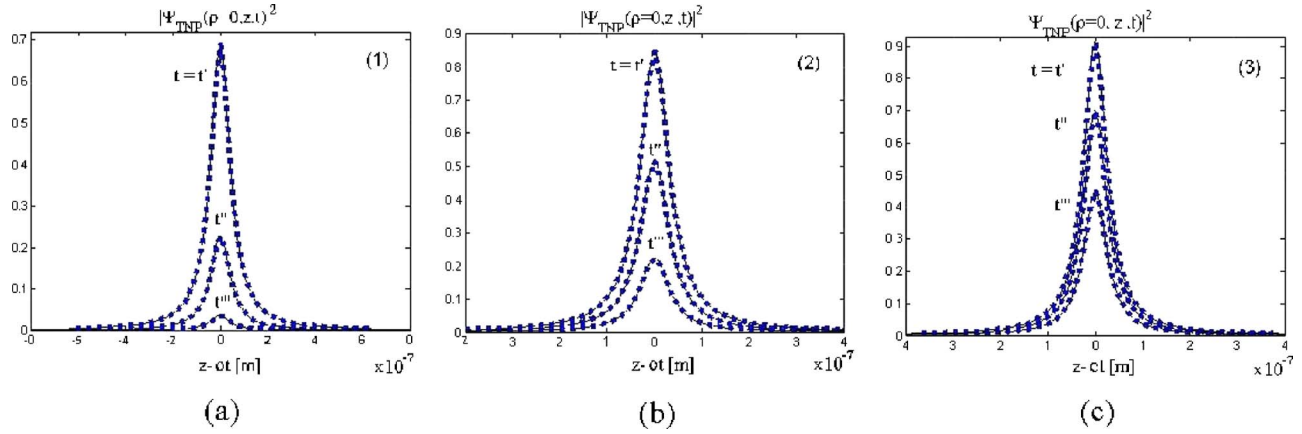

Fig. 5. On-axis evolution of the truncated luminal FWM pulse, at the times $t'=0.22$ ns, $t''=0.44$ ns, and $t'''=0.66$ ns, for each of the cases cited in Fig. 4; (a), (b), and (c) represent cases (1), (2), and (3), respectively. The continuous curves are the results obtained from our closed-form analytical expression (25), and dotted curves represent results from the numerical simulation of the Rayleigh–Sommerfeld formula (8).

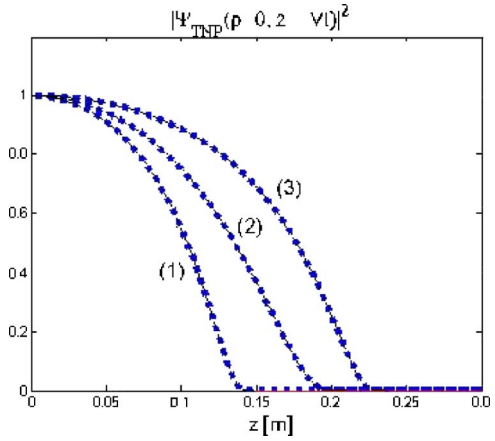

Fig. 6. Peak intensity evolution of the truncated superluminal FWM pulse for the three cases: (1) $V=1.0002c$, $b=3\times10^{12}$ Hz, and $a=2.5\times10^{-17}$ s; (2) $V=1.0001c$, $b=1\times10^{12}$ Hz, and $a=5\times10^{-17}$ s; and (3) $V=1.00008c$, $b=2\times10^{12}$ Hz, and $a=1.1\times10^{-17}$ s. In all cases $R=3$ mm. The continuous curves are results obtained from our closed-form, analytical expression (28), and dotted curves represent results from the numerical simulation of the Rayleigh–Sommerfeld formula (8).

(8). Once more, there is an excellent agreement among the results, confirming the validity and efficiency of our method.

4. EXTENDING THE PRESENT METHOD TO THE ALMOST NONDIFFRACTING (FINITE-ENERGY) PULSES, TRUNCATED BY FINITE APERTURES

In the previous sections we have developed a (heuristic) method capable of providing closed-form analytical expressions, describing the on-axis evolution of the INP truncated by finite apertures. It is well known[1,6] that besides the INPs, there are the almost-nondiffracting pulses (ANPs), which also need infinite apertures to be generated but possess a finite energy content.

Once a function $S(\omega)$ is chosen and an INP with a velocity V and $b=b_0$ is obtained from Eq. (6), we can get an ANP by integrating Eq. (6) over the parameter b with a suitable choice of the weight function $S'(b)$, which has to be concentrated around $b=b_0$. More explicitly,

$$\Psi_{\mathrm{ANP}}(\rho,z,t)=\int_{b_{\min}}^{b_{\max}}\mathrm{d}b\int_{\omega_{\min}}^{\omega_{\max}}\mathrm{d}\omega S''(\omega,b)\times J_0\left(\rho\sqrt{\left(\frac{1}{c^2}-\frac{1}{V^2}\right)\omega^2+\frac{2b\omega}{V^2}-\frac{b^2}{V^2}}\right)\times e^{i\omega\zeta/V}e^{-ibz/V},\tag{29}$$

where $S''(\omega,b)=S(\omega)S'(b)$ is a spectral function with $S'(b)$ well localized around $b=b_0$. Obviously, one can recover the INPs just by adopting the choice $S''(\omega,b)=S(\omega)\delta(b-b_0)$.

An ANP can be viewed as a Bessel beam superposition [Eq. (4)] with a spectral function $\bar{S}(\omega,\beta)$ well concentrated around a straight line $\omega=V\beta+b_0$. The ANPs are interesting solutions, due to their finite-energy contents, and can maintain their spatial shape for long distances.[1,6]

However, even possessing finite energy, the ANPs need—as was said above—infinite apertures in order to be generated, something that cannot be obtained in the real world. Consequently, it is rather important to know the behavior of these pulses when they are truncated by finite apertures—that is, to know the Ψ_{TNP} versions of the Ψ_{ANPs}. These can be obtained by making numerical simulations, again, of the Rayleigh–Sommerfeld integral formula (8), on replacing Ψ_{INP} with Ψ_{ANP}.

On the other hand, the extension of our method to the cases of ANPs truncated by finite apertures can be performed in a very simple way, just by multiplying our fundamental approximations (16), (18), (20), and (21) by the $S(b')$ under consideration and performing the relevant integration over the parameter b. This will be shown by the following example, in which we shall obtain closed-form analytical expressions for the truncated version Ψ_{TNP} of a well-known finite energy ANP,[1,23] namely, the modified power spectrum pulse (MPS).

Example: The truncated version of the MPS pulse. A well-known luminal ANP is the MPS pulse, which can be obtained by integrating, over the parameter b, the FWM pulse (24) with the weight function

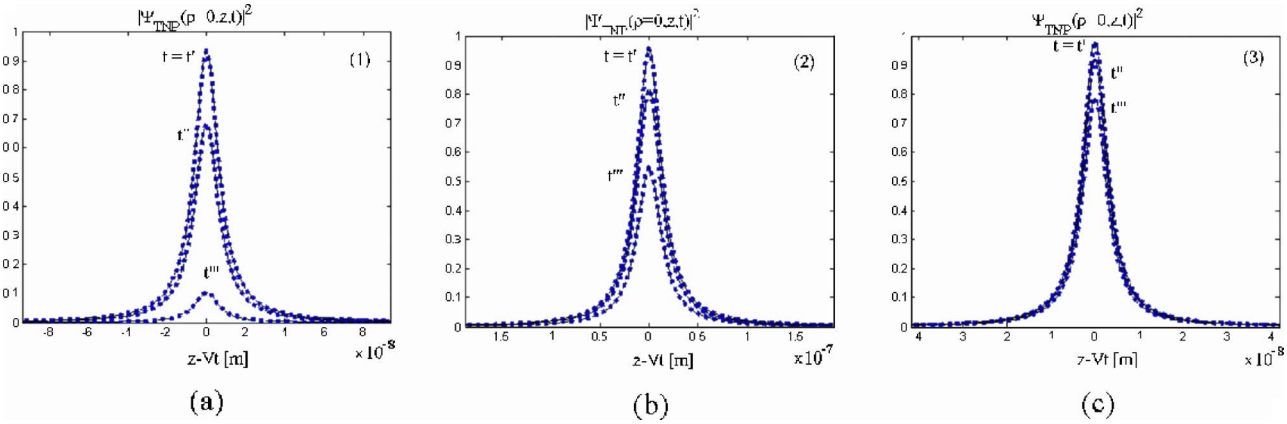

Fig. 7. On-axis evolution of the truncated SFWM pulse, at the times $t'=0.14$ ns, $t''=0.29$ ns, and $t'''=0.43$ ns, for each of the cases cited in Fig. 6; (a), (b), and (c) represent cases (1), (2), and (3), respectively. The continuous curves are the results obtained from our closed-form, analytical expression (28), and results represented by dotted curves come from the numerical simulation of the Rayleigh–Sommerfeld formula (8).

$$S'(b) = H(b-b_0)q\exp[-q(b-b_0)], \tag{30}$$

quantities q and b_0 being positive constants. More explicitly, the MPS pulse can be written as

$$\begin{aligned}\Psi_{\mathrm{ANP}}(\rho,z,t) &= \int_{b_0}^{\infty}\frac{aqc}{ac-i\zeta}\exp\left(\frac{-ib}{2c}\eta\right)\exp\left[\frac{-b\rho^2}{2c(ac-i\zeta)}\right]\\ &\quad\times\exp[-q(b-b_0)]\mathrm{d}b\\ &= \frac{2ac^2q}{(2cq+i\eta)(ac-i\zeta)+\rho^2}\exp\left(\frac{-ib_0}{2c}\eta\right)\\ &\quad\times\exp\left[-\frac{b_0\rho^2}{2c(ac-i\zeta)}\right],\end{aligned} \tag{31}$$

with $\eta=z+ct$, $\zeta=z-ct$. This ANP has a finite-energy content; however, it needs an infinite aperture to be generated.

We shall use the extended version of our method to get a closed-form analytical expression for the on-axis evolution of the truncated version, Ψ_{TNP}, of the MPS pulse. As we have seen, to get this we just need to multiply the truncated version of the FWM pulse, given by approximation (25), by the corresponding weight function $S'(b)$ given by Eq. (30), and perform the integration over the parameter b. In this way, the on-axis evolution of the truncated MPS pulse is given by

$$\begin{aligned}\Psi_{\mathrm{TNP}}(\rho=0,z>0,t) &\simeq \int_{b_0}^{\infty}\frac{aqc}{ac-i\zeta}e^{ab/2}e^{-ibz/c}\\ &\quad\times\exp[-q(b-b_0)]\exp\left[\frac{-b\sqrt{z^2+R^2}(ac-i\zeta)}{c(\sqrt{z^2+R^2}-z)}\right]\mathrm{d}b\\ &= \frac{aqc\,e^{ab_0/2}\,e^{-ib_0z/c}}{(ac-i\zeta)\left[q-\frac{a}{2}+\frac{iz}{c}+\frac{\sqrt{z^2+R^2}(ac-i\zeta)}{c(\sqrt{z^2+R^2}-z)}\right]}\\ &\quad\times\exp\left[-\frac{b_0\sqrt{z^2+R^2}(ac-i\zeta)}{c(\sqrt{z^2+R^2}-z)}\right],\end{aligned} \tag{32}$$

which is a closed-form analytical expression.

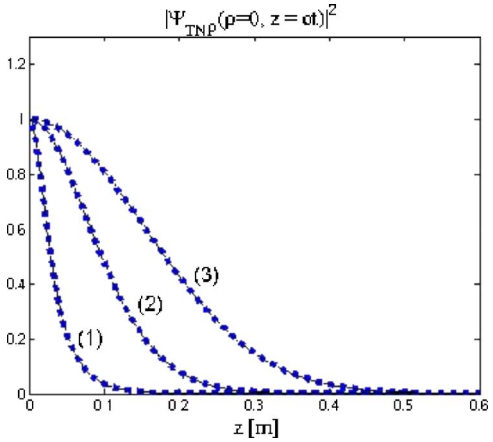

Fig. 8. Peak-intensity evolution of the truncated luminal MPS pulse for the three cases: (1) $a=1.6\times10^{-16}$, $b_0=5\times10^{11}$ Hz, and $q=2\times10^{-11}$ s; (2) $a=1.25\times10^{-16}$ s, $b_0=3\times10^{11}$ Hz, and $q=10\times10^{-11}$ s; and (3) $a=1\times10^{-16}$, $b_0=2\times10^{11}$ Hz, and $q=20\times10^{-11}$ s. In all cases $R=2$ mm. The continuous curves are results obtained from our closed-form analytical expression (32), and dotted curves represent results from the numerical simulation of the Rayleigh–Sommerfeld formula (8).

As before, let us put $\zeta=0$ in approximation (32) to get the pulse peak intensity behavior.

Let us consider three different cases: (1) $a=1.6\times10^{-16}$ s, $b_0=5\times10^{11}$ Hz, and $q=2\times10^{-11}$ s; (2) $a=1.25\times10^{-16}$ s, $b_0=3\times10^{11}$ Hz, and $q=10\times10^{-11}$ s; and (3) $a=1\times10^{-16}$ s, $b_0=2\times10^{11}$ Hz, and $q=20\times10^{-11}$ s. In all cases, we adopt the aperture radius $R=2$ mm.

Figure 8 shows the results. The continuous curves represent those obtained from approximation (32), and the dotted ones are the results of the numerical simulation of the Raleigh–Sommerfield integral formula (8). One can verify the excellent agreement among the results.

Now, we are going to use approximation (32) to investigate the on-axis evolution of this TNP in the three cases considered above for the instants $t'=0.22$ ns, $t''=0.44$ ns, and $t'''=0.66$ ns. Figures 9(a)–9(c) show the results corresponding to cases (1), (2), and (3), respectively. The continuous curves come from approximation (32) and the dotted curves are those coming from the numerical simulation of Eq. (8). Again, we consider $R=2$ mm. Once

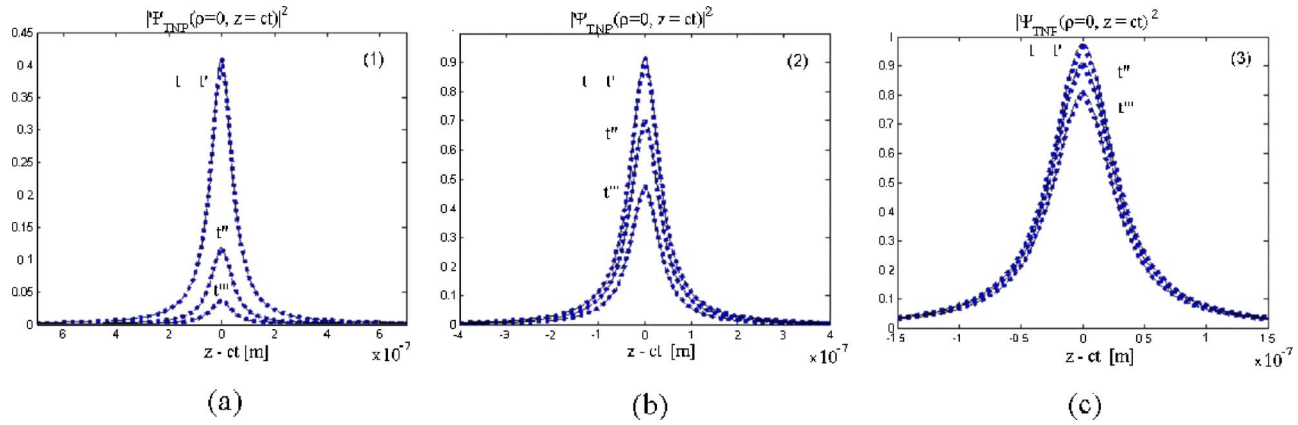

Fig. 9. On-axis evolution of the truncated luminal MPS pulse, at the times $t'=0.22$ ns, $t''=0.44$ ns, and $t'''=0.66$ ns, for each of the three cases considered in Fig. 8; (a), (b), and (c) represent cases (1), (2), and (3), respectively. The continuous curves are the results obtained from our closed-form analytical expression (32), dotted curves represent results from the numerical simulation of the Rayleigh–Sommerfeld formula (8).

more, there is an excellent agreement among the results, confirming the validity and efficiency of our method.

Before finishing this section, it is important to note that the closed-form analytical expressions of the truncated ANP obtained with our method can be used advantageously for comparison purposes with the corresponding nontruncated ANP, thus illustrating the effects due to the truncation and, for example, telling us up to what distance we can use the three-dimensional (3D) solution of the ANP as a good approximation to the corresponding 3D TNP.

5. CONCLUSIONS

In this paper a very simple method has been developed for describing the space–time on-axis evolution of truncated nondiffracting pulses, be they subluminal, luminal, or superluminal. It is important to notice that in this method, given by approximations (16), (18), (20), and (21), the on-axis evolution of a TNP depends only on the frequency spectrum $S(\omega)$ of its corresponding INP Ψ_{INP}, contrary to the Rayleigh–Sommerfeld formula (8), which depends on the explicit mathematical expression of Ψ_{INP}. We also have extended our method to describe the truncated versions of the ANPs. Due to such a simplicity, we can obtain closed-form analytical expressions, which describe the on-axis evolution of innumerable TNPs. In this paper we have done that for the truncated versions of a few, very well-known localized waves: subluminal, luminal or superluminal. We have compared our results with those obtained through the numerical simulation of the Rayleigh–Sommerfeld integrals, and we have observed an excellent agreement among them, confirming the efficiency of our method.

The present approach can be very useful, because it furnishes, in general, closed-form analytical expressions, avoiding the need for time-consuming numerical simulations, and also because such expressions provide a powerful tool for exploring several important properties of the truncated localized pulses such as their depth of field, the longitudinal pulse behavior, and the decaying rates.

ACKNOWLEDGMENTS

The author is very grateful to Erasmo Recami, Hugo E. Hernández-Figueroa, and Claudio Conti for continuous discussions and kind collaboration. Thanks are also due to Jane M. Madureira. This work was supported by Fundação de Amparo à Pesquisa do Estado de São Paulo (FAPESP) (Brazil).

E-mail address: mzamboni@dmo.fee.unicamp.br.

The author is also with the Center of Natural Sciences, Federal University of ABC (UFABC), Santo André, SP, Brazil.

REFERENCES AND NOTES

1. I. M. Besieris, A. M. Shaarawi, and R. W. Ziolkowski, "A bi-directional traveling plane wave representation of exact solutions of the scalar wave equation," J. Math. Phys. **30**, 1254–1269 (1989).
2. J.-y. Lu and J. F. Greenleaf, "Nondiffracting X-waves: exact solutions to free-space scalar wave equation and their finite aperture realizations," IEEE Trans. Ultrason. Ferroelectr. Freq. Control **39**, 19–31 (1992).
3. J. Fagerholm, A. T. Friberg, J. Huttunen, D. P. Morgan, and M. M. Salomaa, "Angular-spectrum representation of nondiffracting X waves," Phys. Rev. E **54**, 4347–4352 (1996).
4. P. Saari and K. Reivelt, "Evidence of X-shaped propagation-invariant localized light waves," Phys. Rev. Lett. **79**, 4135–4138 (1997).
5. E. Recami, "On localized X-shaped superluminal solutions to Maxwell equations," Physica A **252**, 586–610 (1998).
6. M. Zamboni-Rached, E. Recami, and H. E. Hernández-Figueroa, "New localized superluminal solutions to the wave equations with finite total energies and arbitrary frequencies," Eur. J. Phys. **21**, 217–228 (2002).
7. M. A. Porras, S. Trillo, C. Conti, and P. Di Trapani, "Paraxial envelope X-waves," Opt. Lett. **28**, 1090–1092 (2003).
8. G. Nyitray and S. V. Kukhlevsky, "Distortion-free tight confinement and step-like decay of fs pulses in free space," arXiv:physics/0310057vl, Oct. 13, 2003.
9. M. Zamboni-Rached, H. E. Hernandez-Figueroa, and E. Recami, "Chirped optical X-type pulses," J. Opt. Soc. Am. A **21**, 2455–2463 (2004).
10. J. W. Goodman, *Introduction to Fourier Optics* (McGraw-Hill, 1968).
11. R. W. Ziolkowski, I. M. Besieris, and A. M. Shaarawi,

"Aperture realizations of exact solutions to homogeneous wave-equations," J. Opt. Soc. Am. A **10**, 75–87 (1993).
12. J.-y. Lu and J. F. Greenleaf, "Experimental verification of nondiffracting X-waves," IEEE Trans. Ultrason. Ferroelectr. Freq. Control **39**, 441–446 (1992).
13. J.-y. Lu, H.-h. Zou, and J. F. Greenleaf, "Biomedical ultrasound beam forming," Ultrasound Med. Biol. **20**, 403–428 (1994).
14. M. Zamboni-Rached, A. Shaarawi, and E. Recami, "Focused X-shaped pulses," J. Opt. Soc. Am. A **21**, 1564–1574 (2004).
15. This paper first appeared as e-print arXiv:physics/0512148vl, Dec. 16, 2005
16. J. Durnin, J. J. Miceli, and J. H. Eberly, "Diffraction-free beams," Phys. Rev. Lett. **58**, 1499–1501 (1987).
17. M. Zamboni-Rached, "Stationary optical wave fields with arbitrary longitudinal shape by superposing equal frequency Bessel beams: Frozen Waves," Opt. Lett. **12**, 4001–4006 (2004).
18. M. Zamboni-Rached, E. Recami, and H. Figueroa, "Theory of 'frozen waves:' modeling the shape of stationary wave fields," J. Opt. Soc. Am. A **22**, 2465–2475 (2005).
19. M. Zamboni-Rached, "Diffraction-attenuation resistant beams in absorbing media," Opt. Express **14**, 1804–1809 (2006). (Also available as e-print arXiv:physics/0506067v2 Jun. 15, 2005).
20. S. V. Kukhlevsky and M. Mechler, "Diffraction-free sub-wavelength beam optics at nanometer scale," Opt. Commun. **231**, 35–43 (2004).
21. Interesting approximate analytical descriptions for special cases of truncated nondiffracting *beams* (not pulses) are discussed in Z. Jiang, "Truncation of a two-dimensional nondiffracting cos beam," J. Opt. Soc. Am. A **14**, 1478–1481 (1997).
22. A. G. Sedukhin, "Marginal phase correction of truncated Bessel beams," J. Opt. Soc. Am. A **17**, 1059–1066 (2000).
23. R. Donnelly and R. W. Ziolkowski, "Designing localized waves," Proc. R. Soc. London, Ser. A **440**, 541–565 (1993).